Hindawi
Geofluids
Volume 2022, Article ID 4303681, 12 pages
https://doi.org/10.1155/2022/4303681

Research Article

Analysis on Evolution Law of Small Structure Stress Arch and Composite Bearing Arch in Island Gob-Side Entry Driving

Shunjie Huang[1,2], **Xiangqian Wang**[1,2], **Yingming Li**[1,2], **Lei Wang**[3], **Gang Liu**[4], **Fukun Xiao**[4] **and O. V. Bashkov**[5]

[1]*State Key Laboratory of Mining Response and Disaster Prevention and Control in Deep Coal Mines, Anhui University of Science and Technology, Huainan 232001, China*
[2]*School of Mining Engineering, Anhui University of Science and Technology, Huainan, Anhui 232001, China*
[3]*Mining Products Safety Approval and Certification Center Co., Ltd., Beijing 100013, China*
[4]*Heilongjiang Ground Pressure and Gas Control in Deep Mining Key Laboratory, Heilongjiang University of Science and Technology, Harbin 15002, China*
[5]*Komsomolsk-na-Amure State Technical University, Komsomolsk-na-Amure 681013, Russia*

Correspondence should be addressed to Xiangqian Wang; 1203259514@qq.com

Received 11 November 2021; Revised 3 May 2022; Accepted 14 May 2022; Published 23 June 2022

Academic Editor: Zhijie Wen

Copyright © 2022 Shunjie Huang et al. This is an open access article distributed under the Creative Commons Attribution License, which permits unrestricted use, distribution, and reproduction in any medium, provided the original work is properly cited.

At present, the theory of supporting the surrounding rock small structure of gob-side entry driving has been widely used, but there is no specific quantitative analytical formula for the bearing strength and bearing characteristics of the structure. Construct a small structural stress arch mechanical model based on the arch axis equation, and divide the width of coal pillars (fractured zone-plastic softening zone-plastic hardening zone) and small structural stress arch height. According to the relationship between the stress arch height and the size of the roadway, the anchor cable length is determined to be 7.3 m, and the "anchor mesh + ordinary long anchor cable + grouting anchor cable" coordinated support plan is proposed: anchor net support is used for the first support, and long anchor cable and grouting anchor cable are used for the second support. Combined with the supporting parameters, a mechanical model of the surrounding rock composite bearing stress arch is proposed, and the composite bearing stress arch structure is derived using elastoplastic mechanics to obtain the ultimate bearing strength relationship expression. The results show that the ultimate bearing capacity of the haulage gateway of 17236 island working-face in the north of Zhangji coal mine can reach 29.193 MPa after the composite bearing stress arch support. The feasibility of the supporting scheme is verified, and field monitoring showed that the deformation zone of the surrounding rock of the transportation haulage gateway is stable after being supported by the composite bearing stress arch structure, the maximum shrinkage of the top and bottom of the roadway is 287 mm, and the distance between the two sides is 640 mm.

1. Introduction

At present, many mines have entered the residual mining stage due to the rapid decline of recoverable reserves of coal resources due to high tension coal mining, in order to improve the recovery rate of coal resources and prolong the production and service life of mines, and gob-side entry has become the first choice for island working-face [1–4]. Under the action of side abutment pressure of gob-side entry in isolated island working-face, the roof pressure is big, the degree of coal fragmentation is high, the difficulty of roadway support is improved, and the roadway damage is serious due to mining influence and geological structure [5–9].

Therefore, the support of gob roadway is particularly important for island face mining. Wang et al. [10] analyzed the deformation mechanism and the stress state of gob-side entry driving heading adjacent to the advancing working-face (HAWF) roof structure and proposed a roof failure criterion to examine the roof flexure deformation pattern. Zhang et al. [11] analyzed the distribution law of lateral support stress near the working-face, discussed the relationship between coal pillar stress distribution and coal pillar

deformation, roadway surrounding rock stress distribution, roadway surrounding rock deformation, and coal pillar width, and verified the feasibility of coal pillar width through the field. Ma and Zhong [12] established the "three zone" failure similarity simulation experimental model of surrounding rock and deduced the action mode of surrounding rock stress structure, but there is no theoretical and numerical simulation analysis and lack of theoretical basis. Hou and Li [13] analyzed the mechanical properties of arc triangular key blocks of the main roof, put forward the stability principle of big and small structures, and provided a theoretical basis for the application of bolt support. Yang et al. [14] regard the broken rock mass near the roadway opening as a small ground structure and the deep stable rock mass as a big ground structure through numerical simulation software experiments and proposed support technology of interconnecting the big and small structures, based on high-strength bolts, high-stiffness shotcrete layer plugging water, and strengthening the small structure with deep-hole grouting. Wu et al. [15] established the three-dimensional structural mechanics model of deep stope, put forward the "big and small structure theory" of coal pillar free mining, and found a new method to control the two tunnel dynamic disasters of "given deformation" and "finite deformation." Zhang et al. [16] proposed a new joint support technology in the soft rock roadway of Gubei Coal Mine in Huainan, China. The on-site monitoring results show that the combined support technology is satisfactory. Li and Hua [17] put forward a supporting concept of enhancing the support strength and realizing the cutting roof and designed three roadside support schemes of gob-side entry for a soft floor and hard roof.

Most of the current research results focus on the "big-structure" of gob-side entry driving; however, the research on the small structure of surrounding rock of gob side roadway with isolated coal pillar mostly ignores the arch height of small-structure stress and the bearing strength of roadway support structure. Zhao et al. [18] analyzed the evolution of stress arch through theoretical and numerical simulation, and a zoning asymmetric coupling control technology named narrow flexible-formwork wall with steel bar reinforcement along single prop wall + strong double-row single props + high-strength and high-preloading asymmetric anchor cable is proposed. For the small structure of surrounding rock of roadway along working-face of isolated island coal pillar, the arch height of small structure stress and the bearing strength of roadway support structure are mostly ignored. Therefore, according to the structural characteristics of surrounding rock of gob driving roadway, the coal pillar failure area is divided into fractured zone-plastic softening zone-plastic hardening zone [19–37] and according to the total stress-strain curve. Taking the gob driving roadway of isolated island working-face of the north of Zhangji coal mine as the research background, the anchor cable support parameters and the bearing strength of "composite bearing stress arch" structure formed by the support structure and surrounding rock are calculated through theoretical analysis. The corresponding support scheme is adopted for field industrial test, and the reliability of the support scheme is verified.

2. Background

2.1. Geological Conditions. The schematic diagram of 17236 working-face in the north of Zhangji coal mine of Huaihe Energy Coal Industry Company is shown in Figures 1 and 2. It is located between 17226 working-face and 17246 working-face. The mine able strike length of 17236 island working-face is 1580 m (horizontal range), and the elevation of the working-face is -519.6~-630.0 m. A narrow coal pillar of 8 m is reserved along the edge of 17246 working-face. The design section of the roadway is rectangular, with a net section zone of 18.7 m^2, an average dip angle of 4.5°, and an average thickness of 4.2 m. The direct top is sandy mudstone with an average thickness of 3.8 m, and the direct bottom is silty fine sandstone with an average thickness of 1 m; the surrounding rock column diagram is shown in Figure 3.

2.2. The Failure Characteristics of Gob-Side Entry Driving. The stress field of the transportation trough of 17236 island working-face based on lateral bearing pressure and advance bearing pressure in Zhangji North Mine was found through field study. The rock pressure appeared mainly shows the failure forms of roadway: bolt and anchor cable fractured, steel belt broken and cracked, and steel beam bent and deformed, which seriously affects the safety and stability of roadway. The failure characteristics of roadway are shown in Figure 4.

And four roadway section monitoring points (each monitoring point is 40 m away and 3#, 4# measuring points are located in the abnormal fault development zone) are selected in the haulage gateway 158 m from the cutting hole. The monitoring results are shown in Figure 5. The results show that the displacement of roadway's two side is big, especially at the 3# and 4# measuring points in the abnormal zone. The deformation degree is the biggest, and the maximum deformation rate can reach 47 mm/d. At the same time, the roof shrinkage is serious.

(1) Composition of surrounding rock. The surrounding rock of the roadway is mainly silty fine sandstone, sandy mudstone, and fine sandstone. The rock strength test is carried out on the samples taken from the top and bottom plates. It can be seen that the compressive strength of fine sandstone and sandy mudstone is 26.6 MPa and 15.8 MPa, respectively, and the compressive strength of silty fine sandstone is 23.9 MPa. The rock mass has low load resistance. Under the condition of high stress intensity, the surrounding rock fissures develop violently, and the expansion deformation is big

(2) Mining depth. The buried depth of the haulage gateway is 653 m, with big in situ stress and unstable surrounding rock

(3) Mining method. When the skip mining method is adopted for mining, the surrounding rock is disturbed, resulting in the deterioration of the integrity and bearing capacity of the roadway surrounding rock, leading to the advance of the crushing range

Figure 1: Location of the north of Zhangji coal mine.

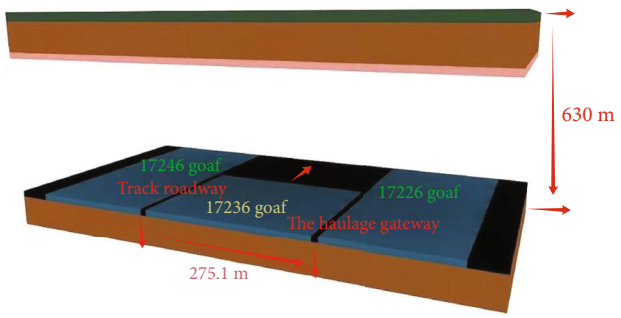

Figure 2: Schematic diagram of position relationship of 17236 working-face.

Lithology	Columnar	Thickness (m)
Mudstone		1.7
Coal line		0.5
Sandy mudstone		2.1
Fine sandstone		2.8
Sandy mudstone		3.8
6 coal		4.2
Siltstone		1
Coal line		0.4
Siltstone		1.6
Medium grained sandstone		4.1

Figure 3: Synthesis column map of the surrounding rock.

of the working-face, affecting the transportation channel, and increasing the instability of the roadway

(4) The superposition of excavation disturbance and residual mining stress has a serious impact. Due to the big buried depth of the roadway and the superposition of the vertical stress and the residual mining

Figure 4: Deformation and failure characteristics of roadway surrounding rock.

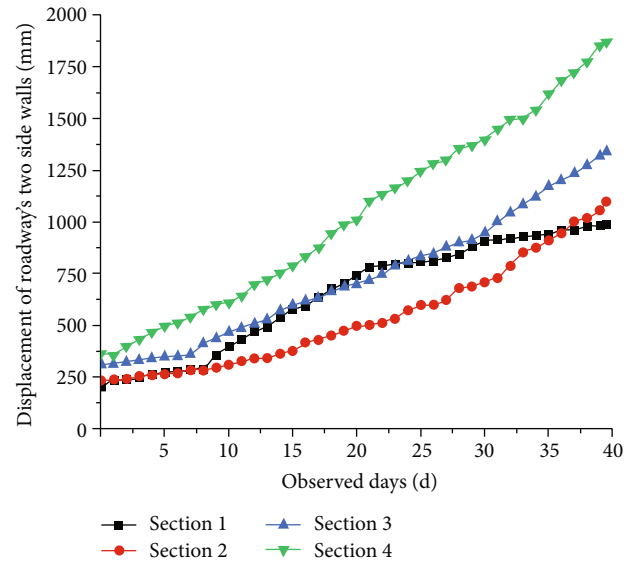

Figure 5: Convergence of the haulage gateway.

stress in the working-face, the peak strength of the coal body is low

According to the above analysis, in order to solve the problem that the roof separation and roadway side deformation become the core of the support technology, the bolt group is generally used for intensive support in the early stage, which can provide great support resistance within the anchorage range, but the surrounding rock outside the bolt length will still produce separation, resulting in roof caving. Therefore, only by improving the support structure and strengthening the support technology can the roadway deformation be minimized.

Therefore, in order to better act the nonanchored rock mass load and the expansion energy generated by the broken rock mass on the bolt in the early stage of the roadway, the metal mesh can be added to the original bolt support mode to control the deformation of the nonanchored rock mass and prevent the collapse of the broken rock mass. At the same time, in order to further improve the service life of roadway and the bearing capacity of narrow coal pillar, in the later stage, in order to mobilize the bearing energy of deep surrounding rock and narrow coal pillar, grouting anchor cable and long anchor cable can be added for joint support, improve the stress state of surrounding rock, and effectively control the deformation of roadway surrounding rock.

3. Stability Analysis of Overburden Stress Arch along Gob-Side Entry in Isolated Island Working-Face

3.1. Mechanical Model of Overburden Stress Arch along Gob-Side Entry in Isolated Island Working-Face. With the completion of the previous excavation working face, the overlying rock on the roof of the goaf collapses, and the rock blocks after the periodic rupture of the basic roof or the old roof will follow the direction or inclination of the working face, and the overlying rock in the goaf will inevitably form a large structure. Among them, the artificial support has little effect on the large structure, but the artificial support mainly controls the stability of the small structure under the large structure.

After the mining disturbance of the gob-side roadway, the overlying rock mass structure will be stable in the form of stress arch (the arch line trajectory belongs to the distribution law of the envelope curve under the Moore-Coulomb criterion strength) and form a "large-small" structure to protect the coal and rock below body and roadway. The large structure is a large-scale surrounding rock structure with coal pillars and arc-shaped triangular blocks as the main centers, but the small structure usually takes the roadway as the center point and the "support-surrounding rock" system becomes a small bearing structure. Among them, the small structure is under the large structure, and the arch foot is close, the stability of the large structure determines the stability of the small structure, and at the same time, the stability of the small structure affects the stability of the arch foot, thus affecting the stability of the large structure; "small" structures interact and influence each other. The schematic diagram of the "big-small" structure is shown in Figure 6. Since the key block with the greatest influence on the stability of the gob-side roadway is block B, this chapter studies the influence of block B on the small structure of the gob-side roadway after stabilization [15–19].

The small structure of the gob-side entry is an arch structure [20–22]. The arch foot of the arch is located on both sides of the solid coal and the coal pillars, and the apex of the arch is located at the point of stress concentration. For better analysis of the stress arch height, referring to the solution method of literature [23] for analysis, the internal stress distribution of the coal pillar is analyzed separately, and it will correspond to the whole stress-strain curve. The failure area of the arch foot is from the flow zone of the coal pillar (close to the working-face side) and the plastic softening zone to the junction of plastic hardening zone and elastic zone (K is the stress concentration factor of coal pillar; γ is the unit weight of overburden (kN/m^3); H is the mining depth of coal seam (m); x_f is the width of fractured zone (m); x_s is the width of plastic softening zone (m); x_e is the width of plastic hardening zone (m)).

According to the above, the arch foot is located at the junction of the flow zone and the plastic softening zone. Therefore, the arch axis mechanical model is established. In order to facilitate the analysis, the following assumptions are made for the model: (1) given deformation of curved triangle block B and the block is stable; (2) the arch structure can be approximately regarded as a horizontal semicircular arch, and the arch thickness remains unchanged; (3) the stress arch apex is vertically corresponding to the roadway center point; the arch foot is horizontally symmetrical; (4) the rock mass still has cohesion after excavation; (5) arch structures only bear compressive stress but not tensile stress, and the mechanical model is shown in Figure 7.

Set the arch axis equation as:

$$\frac{x^2}{(S)^2} + \frac{y^2}{(H_g)^2} = 1, \quad S = 2r + 2x_e. \tag{1}$$

In the formula, S is the arch span (m); P_0 is the gravity of overlying strata (MPa); H_g is the arch height (m); F_{Ax}, F_{Ay}, F_{BX}, and F_{By} are the reaction force (MPa) of arch foot at two points A (solid coal) and B (coal pillar); G_X is the horizontal force of the right half arch to the left half arch (MPa); R is the distance from the roadway center to a certain point of surrounding rock (m).

From the model of mechanical equilibrium equation in the Y direction, it can be obtained:

$$F_{Ay} = F_{By} = \frac{P_0 S}{2}. \tag{2}$$

From formula (3), it can be seen that the arch foot bears a great load in the vertical direction. In order to meet the stability of the arch foot in the vertical direction, the plastic

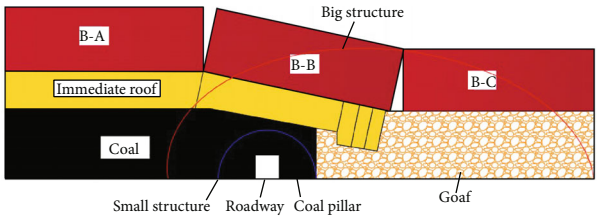

Figure 6: Schematic diagram of big and small structure of surrounding rock in gob-side entry driving.

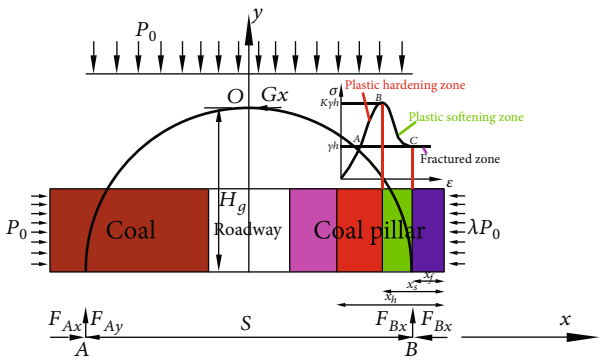

Figure 7: Mechanical model of stress arch (small-structure).

softening zone, plastic hardening zone, and elastic zone are arch feet. According to the literature [24, 25], the results are as follows.

The width of the fractured zone is:

$$x_f = \frac{2h\left[\tan^2(45^\circ - (\varphi_e^*/2)) - (P_0/\gamma H)\right]}{(\tan\varphi_{eu}^* + \tan\varphi_{ed}^*)}. \tag{3}$$

The width of the coal gang destruction zone is:

$$x_s = \frac{2h\left[\tan^2(45^\circ - (\varphi_{se}^*/2)) - (P_0/\gamma H)\right]}{(\tan\varphi_{su}^* + \tan\varphi_{sd}^*)}. \tag{4}$$

The width of the limit equilibrium zone is:

$$x_h = \frac{L\lambda}{2\tan\varphi^*}\ln\left(\frac{K\gamma H + (c_0/\tan\varphi^*)}{(c_0/\tan\varphi^*) + (P_0/\lambda)}\right). \tag{5}$$

From the above formula, c_0 is the comprehensive cohesion of stress arch bearing structure (MPa); φ^* is the comprehensive internal friction angle of stress arch bearing structure (°); L is the roadway side height (m); φ^*_e is the friction angle in the coal seam in the fractured zone (°); φ^*_{se} is the comprehensive internal friction angle of coal seam in fractured zone and plastic softening zone (°); φ^*_{eu} is the angle of internal friction between the coal seam and the roof in the fracture zone (°); φ^*_{su} is the integrated internal friction angle between the coal seam and the roof in the fracture zone and plastic softening zone(°); φ^*_{ed} is the angle of internal friction between the coal seam and the base plate in the fractured zone (°); φ^*_{sd} is the integrated angle of internal friction between the coal seam and the base plate in the fractured zone, plastic softening zone (°).

Within the plastic softening zone $[x_f, x_s]$, the stress is distributed as follows:

$$\sigma_{y1} = \gamma H - \frac{x - x_f}{x_s - x_f}(1 - K)\gamma H. \tag{6a}$$

Similarly, within the plastic hardening zone $[x_s, x_h]$, the stress is distributed as follows:

$$\sigma_{y2} = \gamma H - \frac{x_h - x}{x_h - x_s}(1 - K)\gamma H. \tag{6b}$$

The derivation of the integral for each partition range of Equations (6a) and (6b) above gives:

$$\left.\begin{aligned} F_{Ay1} &= \frac{(x_s - x_f)(K+1)\gamma H}{2} \\ F_{Ay2} &= \frac{(x_h - x_s)(K+1)\gamma H}{2} \end{aligned}\right\}. \tag{7}$$

Taking the left half-arch as the object of study and taking the moment formula for the rotation axis O, we can obtain:

$$-H_g F_{Ax} - \frac{1}{2}\left(\frac{S}{2}\right)^2 P_0 - \frac{H_g^2}{2}\lambda P_0 + \frac{L_s}{2}F_{Ay} = 0. \tag{8}$$

According to the Morh-Coulomb, the shear stress between the top and bottom slab and the coal body is:

$$\tau_x = c_0 + \sigma_y \tan\varphi^*, \tag{9}$$

where c_0 is the cohesive force at the interface between the roof and floor and the coal seam(MPa); φ^* is the angle of internal friction at the interface between the roof and floor and the coal seam (°).

From Equation (10), it can be seen that the shear stress τ_x is related to the size of the coal pillar stress φ_y, so the coal pillar stress φ_y satisfies:

$$\sigma_y = F_{y1} + F_{y2}. \tag{10}$$

At the same time, simultaneously, Equations (6a), (6b), (9), and (10) into Equation (11), the result is the horizontal friction force F_f at the foot of the arch:

$$F_f = \int_{x_f}^{x_h} \tau_x dx. \tag{11}$$

Simultaneous Equations (7)~(11), the analytical expression of stress arch structure height H_g is as follows:

$$H_g = \frac{\left(-2F_f + \sqrt{4F_f^2 + \lambda[SH\gamma]^2}\right)}{2\lambda H\gamma}. \tag{12}$$

From Equation (12) it can be seen that horizontal friction force F_f, measurement coefficient λ, appearance density γ, and burial depth H all have an influence on the stress arch height. And the horizontal friction force at the arch foot is located in the coal pillar plastic zone (as shown in Figures 5 and 6), the stress value here is the biggest, and the plastic softening zone and plastic hardening zone of coal pillar are superimposed on the plastic zone formed by roadway surrounding rock of roadway, the extent of rock mass failure continues to increase over time, while the failure range of rock mass is within the height of the stress arch. Therefore, it is necessary to select the optimal supporting parameters to effectively and reasonably control the development of the damage zone.

3.2. Example Analysis of Test Roadway. In order to verify the above theoretical analysis, according to the actual occurrence of surrounding rock along the 17236 transport channel in Zhangjibei Coal Mine and the rock mechanical test results, the experimental result is arch span $S = 21.5$ m, mining depth $H = 653$ m, stress concentration factor $K = 2.8$ and measurement coefficient $\lambda = 0.3$, overlying rock capacity = 25 kN/m^3, overlying strata load P0 = 18 MPa, comprehensive cohesion $c0 = 1.8$ MPa, combined internal friction angle $\varphi^* = 25°$, and $\varphi^*_e = 20°$, $\varphi^*_{eu} = 19°$, $\varphi^*_{ed} = 22°$, $\varphi^*_{se} = 16°$, $\varphi^*_{su} = 15°$, and $\varphi^*_{sd} = 17°$, the above parameters are substituted into Equations (3)~(5), (7)~(8), (10), and (13) to obtain the partition width of gob-side entry and the stress arch height along the roadway.

3.3. Selection of Roadway Support Parameters. According to Table 1, it can be concluded that the fractured zone is 2.22 m, plastic softening zone is 2.39 m, and plastic hardening zone is 2.49 m of the coal column in the original support. The stress arch height is 10.738 m, and the thickness of the arch structure is 7.338 m. So, according to the relationship between the arch height of the stress arch and the size of the roadway, the length of the roadway anchor cable is 7.3 m, and it is proposed that the roadway is supported by anchor nets for the first time. The anchor bar is made of left-hand screw steel with length of 2500 mm, diameter of 20 mm, and the spans and rows are both 800 mm, metal mesh protects roadway's roof (5200 × 1000 mm), and metal mesh protects roadway's two side walls (3400 × 1000 mm). The secondary support uses ordinary anchor cable with a length of 7300 mm and diameter of 21.8 mm, and the spans are 1100 mm, and the rows are 800 mm, and grouting anchor cable with a length of 4300 mm, diameter of 22 mm, 17 anchors per row, and 7 anchor cables (two sides are grouting anchor cables) are arranged to suppress the expansion of deformation along the groove side of the track. Single-liquid cement slurry is used for consolidation grouting, with water-cement ratio of 0.6~0.8 : 1 and grouting pressure of 3~8 MPa; the support time node of pillars and roadway solid coal-side can be used as the optimal time for reinforcing roadways by grouting when the initial support roadway deformation is close to the threshold value. The roadway section support diagram is shown in Figure 8.

Table 1: Partition and stress arch height of coal pillar in transportation channel.

Partition category	Thickness/m
Fractured zone	2.22
Plastic softening zone	2.39
Width of coal slope failure zone	4.61
Plastic hardening zone	2.49
Width of limit equilibrium zone	7.1
Arch height (small structure height)	10.738

4. Rational Analysis of Supporting Structure Strength of Test Roadway

4.1. The Structural Strength of Theoretical Analysis. Because the stress area in the arch is mainly composed of the tension stress area of the anchor cable support and the compression stress area of the anchor bar-anchor cable and interacts with the surrounding rock to form the anchor composite bearing body to maintain the roadway stability, in order to verify the rationality of supporting parameters, the structural strength of anchor composite bearing stress arch should be analyzed, and the following assumptions are made in combination with the field geological data of 17236 island working-face:

(1) The surrounding rock of the roadway after support is isotropic and homogeneous, and the anchored composite bearing body is in the broken state of the surrounding rock

(2) The composite bearing structure is completely in contact with the external surrounding rock, and the external load is evenly distributed on the surface of the bearing body

(3) The surrounding rock of the roadway after support is the elastic-plastic medium, and the rock mass follows the Mohr-Coulomb strength criterion

Before the gob-side entry driving excavation, the surrounding rock was already in the nonisocompressive stress field. With the increasing excavation depth, the stress state of the nearby surrounding rock changes from three direction to two direction, and the shallow surrounding rock enters the crushing and plastic state. Through the initial reinforcement of the anchor rod, the anchor area and the surrounding rock combine to form. Before the roadway excavation, the surrounding rock is in the original rock stress field. With the increasing excavation depth, the stress state of the nearby surrounding rock changes from three direction to two direction, and the shallow surrounding rock enters the crushing and plastic state. Through the initial reinforcement of the anchor rod, the anchor anchoring area couples with the surrounding rock to form a secondary bearing layer, which plays a role in supporting the fractured surrounding rock. With the rapid growth of surrounding rock deformation, the surrounding rock is in tension or compression shear state due to the insufficient bolt support strength. When

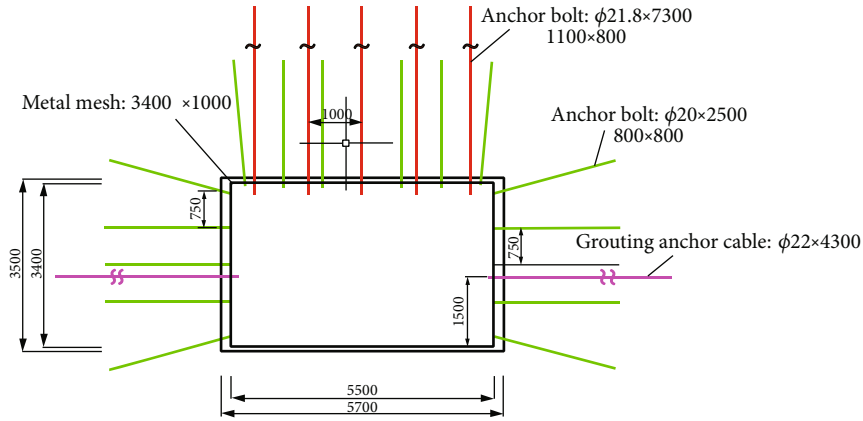

Figure 8: Diagram of roadway support section.

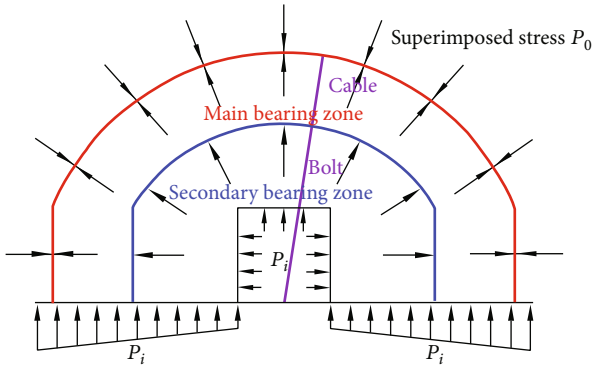

Figure 9: Mechanical model diagram of composite bearing stress arch structure.

the external load exceeds the bearing capacity, the crack initiation and breakthrough appear of the surrounding rock, the anchor structure tends to be broken, and the surrounding rock deformation energy is also released rapidly to inhibit the development of harmful deformation of surrounding rock. The deformation increases gradually, and the surrounding rock surface cracks and heaves, and then sloughs. At this time, the anchor cable can form a new bearing stress structure—main bearing structure in the deep surrounding rock of the roof. In the whole bearing stress structure, the secondary bearing layer formed by the anchor blot groups is connected with the deep surrounding rock through the suspension effect of the anchor cable, to enhance the support effect of the secondary bearing structure and also mobilize the bearing capacity of the main bearing layer, so as to control the deformation of the surrounding rock. The mechanical model diagram of composite bearing stress arch structure is shown in Figure 9.

According to the analysis of the above assumptions, under the limit equilibrium condition of the composite bearing stress arch structure, the surrounding rock after support still follows the Mohr-Coulomb criterion of strength:

$$\sigma_1 = \sigma_3 \frac{1+\sin\varphi_b}{1-\sin\varphi_b} + \frac{2c_b\cos\varphi_b}{1-\sin\varphi_b}, \tag{13}$$

where σ_1, σ_3 is the maximum and minimum principal stress in surrounding rock (MPa); c_b is the cohesion of bearing structure (MPa); φ_b is the internal friction angle of bearing structure (°); therefore, the stress state of a certain point of surrounding rock in the bearing structure meets Equation (14), indicating that the bearing structure is in failure state at this time. Assuming that the surrounding rock stress in the bearing structure is equal to the support resistance, there can be $\sigma_3 = P$, and the support resistance P is:

$$P = P_1^* + P_2^* + P_3^* + P_4^*, \tag{14}$$

where P is the total support resistance (MPa) in support structure and the force in its structure is: P_1^* is the primary support resistance of anchor bolt (MPa); P_2^* is the secondary support resistance of common anchor cable (MPa); P_3^* is the support resistance of metal mesh (MPa); P_4^* is the support resistance of grouting anchor cable (MPa). By substituting the above formula into Equation (14):

$$\sigma_1 = (P_1^* + P_2^* + P_1^* + P_2^*)\cdot\frac{1+\sin\varphi_b}{1-\sin\varphi_b} + \frac{2c_b\cos\varphi_b}{1-\sin\varphi_b}. \tag{15}$$

It can be seen from the above formula that the support resistance affects the maximum principal stress σ_1, the support resistance increases with the principal stress σ_1 increase and become bigger. In order to consider the influence of support parameters on the composite bearing stress arch structure, the underground stress analysis of a certain point of surrounding rock in the bearing structure can be obtained from the static balance equation along the vertical direction of the roadway:

$$F_n = b\sigma_1 + \int_0^b F_{(x)}\mathrm{d}x, \tag{16}$$

where F_n is the bearing force on the arch structure with composite bearing stress (MPa); b is the thickness of composite bearing stress arch structure (m); $F_{(x)}$ is the vertical

Table 2: Physical and mechanical parameters of rock.

Lithology	Density	Bulk modulus (GPa)	Shear modulus (GPa)	Tensile strength (MPa)	Cohesion (MPa)	Friction angle (°)
Mudstone	2382	5.93	4.74	2.74	3.52	28
Sand mudstone	2447	6.68	5.27	3.58	3.2	27
Mudstone	2382	5.93	4.74	2.74	3.52	28
Coal line	1421	3.8	1.63	0.6	1.9	27
Sand mudstone	2312	5.3	4	2.4	2.8	25
Fine sandstone	2335	4.15	3.2	1.5	3.6	34
Sand mudstone	2270	4.76	3.85	1.35	2.5	21
6-coal	1390	4.33	1.77	0.8	1.8	25
Siltstone	2210	6.1	4.79	2.68	3.25	28
Coal line	1265	4.6	3.54	1.13	2.1	26
Siltstone	2286	6.38	5.6	3.26	4.5	31
M-granted sandstone	2080	5.4	4.1	1.89	4.7	35
Sand mudstone	2312	5.3	4	2.4	2.8	25

component function of the radial uniformly distributed load along the composite stress bearing arch structure, that is $F_{(x)} = kx$.

According to the simultaneous Equations (14) (16), the bearing force Fn outside the composite bearing stress arch is:

$$F_n = b\left[\left(P_1^* + P_2^* + P_1^* + P_2^*\right)\cdot\frac{1+\sin\varphi_b}{1-\sin\varphi_b} + \frac{2c_b\cos\varphi_b}{1-\sin\varphi_b}\right] + \frac{kb^2}{2}. \tag{17}$$

Assuming that the composite bearing stress arch is in the limit equilibrium state at this time, $F_n = P$, and considering the symmetry of the bearing arch, that is:

$$\begin{aligned} 2F_n &= \int_0^{\beta} qR\sin\gamma \mathrm{d}\gamma - PB, \\ \beta &= 2\arcsin\left(\frac{(B/2)+b}{R}\right), \end{aligned} \tag{18}$$

where R is the outer boundary radius of composite bearing stress arch structure (m); β is the center angle differential element corresponding to the arc segment d_s.

$$q = \frac{2b\left[\left(P_1^* + P_2^* + P_1^* + P_2^*\right)\cdot\left(1+\sin\varphi_b/1-\sin\varphi_b\right) + \left(2c_b\cos\varphi_b/1-\sin\varphi_b\right)\right]}{R(1-\cos\beta)} + \frac{kb^2}{R(1-\cos\beta)} + \frac{PB}{R(1-\cos\beta)}. \tag{19}$$

Among them, the support strength of anchor bolt (anchor cable) is mainly through the axial action and the use of confining pressure to improve the peak strength and residual strength of surrounding rock, so as to enhance the support strength of rock mass in the anchorage zone.

Therefore, the relationship between the support resistance of anchor blot, anchor cable, and metal mesh and other support parameters [16] is as follows.

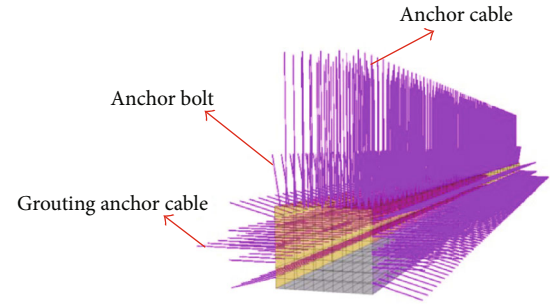

Figure 10: The support structures in numerical model.

The support resistance of anchor blot $P_1{}^*$ is:

$$P_1^* = \frac{P_1}{et}. \tag{20}$$

The support resistance of anchor cable $P_2{}^*$ is:

$$P_2^* = \frac{P_2}{e^* t^*}, \tag{21}$$

where P_1 and P_2 are the axial load of anchor blot and anchor cable (MPa). e and t are the spans and rows of anchor blot (m); e^* and t^* are the spans and rows of anchor cable (m).

The support resistance of metal mesh $P_3{}^*$ is:

$$P_3^* = \frac{2\tau_3 S_3}{2B\cos\left(\pi - 2\varphi_b/4\right)\beta_3}, \tag{22}$$

where τ_3 is the shear strength of the material (MPa); β_3 is the material shear angle (°); S_3 is the cross-sectional area of the metal mesh in the radial direction of the roadway (m^2).

The bearing strength of the composite bearing stress arch structure is obtained from the analysis of Equations (20)~(22), and the structural strength is calculated in combination with the indoor uniaxial compression test and the field geological conditions, The bearing strength of the composite bearing stress arch structure is obtained from the

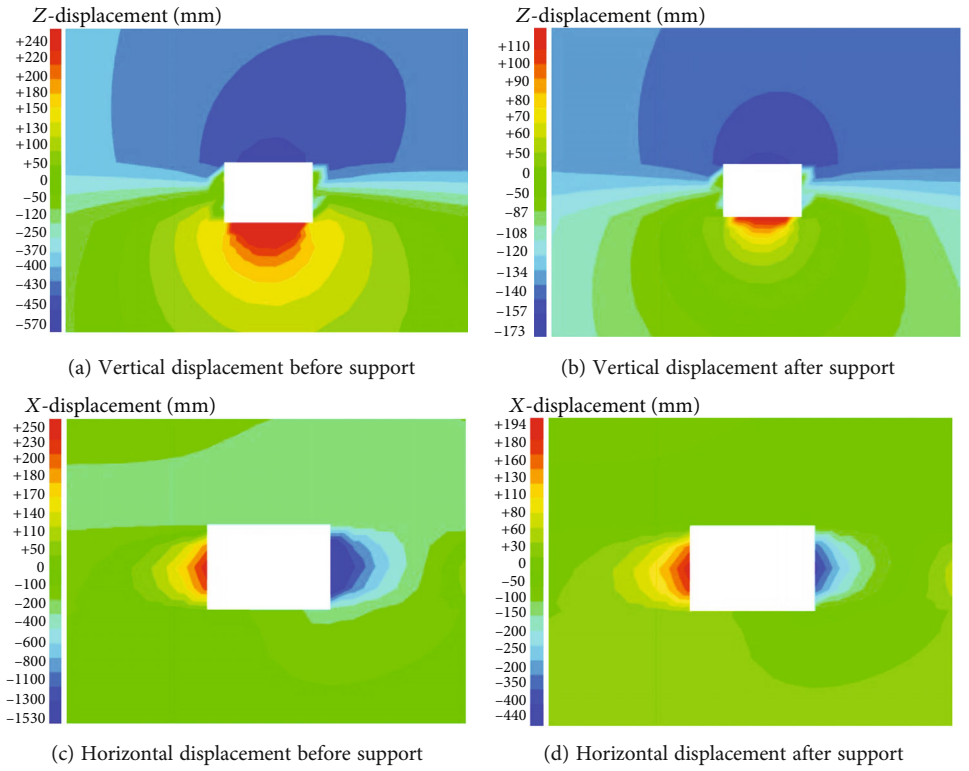

(a) Vertical displacement before support

(b) Vertical displacement after support

(c) Horizontal displacement before support

(d) Horizontal displacement after support

Figure 11: Displacement of roadway before and after support. (a) Vertical displacement before support. (b) Vertical displacement after support. (c) Horizontal displacement before support. (d) Horizontal displacement after support.

analysis of Equations (20)~(22), and the structural strength is calculated in combination with the indoor uniaxial compression test and the field geological conditions, through the calculation of each support structure, the total support resistance $P = 8.63$ MPa, the thickness B of the composite bearing stress arch structure is 7.338 m, the cohesion after support is 2.6 MPa, and the internal friction angle is 30°. By substituting the parameters of rock mass and bearing structure into the above formula, the ultimate bearing capacity of the composite bearing stress arch structure formed after 17236 transportation along the channel support in Zhangji north coal mine is $q = 29.193$ MPa, which is greater than the superimposed stress of 25 MPa, which proves that the composite bearing stress arch structure can maintain the stability of the roadway.

4.2. Numerical Simulation Verification. In order to better verify the reliability of the bolt-anchor cable stress distribution law in the theoretical analysis, the three-dimensional numerical simulation software FLAC3d is used to simulate and verify the geological conditions of the transportation channel in Zhangjibei Coal Mine. The physical and mechanical parameters of the roof and floor of the roadway are shown in Table 2. The surrounding rock is mainly composed of fine sandstone, argillaceous sandstone, and silt fine sandstone. A numerical simulation model is established by the simulation calculation software FLAC3D; the size of the numerical model in X direction, Y direction, and Z direction are 274 m, 300 m, and 100 m; the numerical simulation adopts the Mohr-Coulomb criterion; and the tunnel section

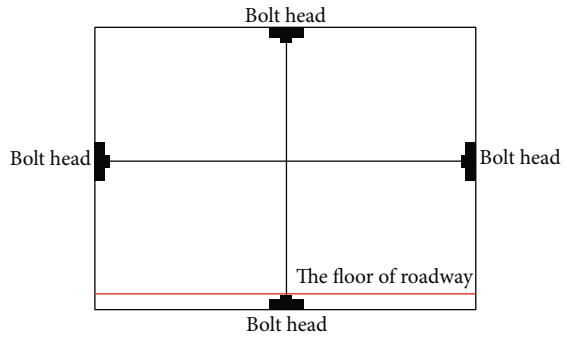

Figure 12: Full section monitoring points of haulage gateway.

Figure 13: Construction site diagram of roadway after support.

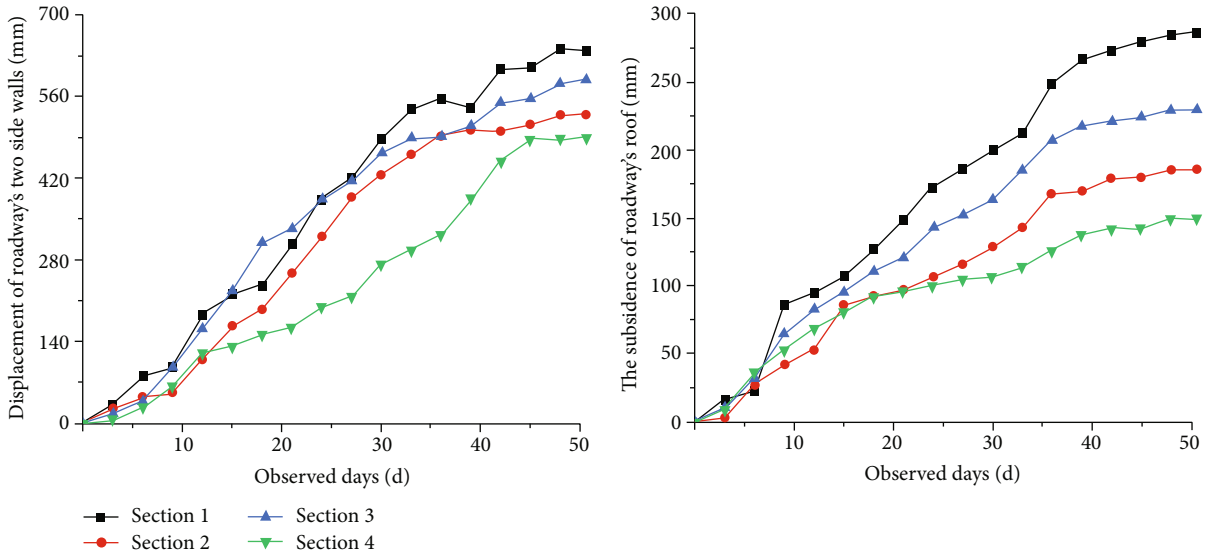

(a) Displacement of roadway's two side walls

(b) The subsidence of roadway's roof

Figure 14: Roadway surface displacement monitoring results.

is rectangular, with a height of 4 m and a width of 5 m. Since the simulated depth of the roadway is 630 m, the average density of the surrounding rock mass is 2500 kg/m^3. Therefore, the ground stress is 15.75 MPa. After the initial stress is balanced, after the working-face is excavated and stabilized, the actual parameters of the roadway are installed with bolts, ordinary anchor cables, and grouting anchor cables. The numerical model diagram of the supporting structure is shown in Figure 10.

The vertical and horizontal displacements of the roadway before and after the support are shown in Figure 11. Due to the influence of the composite stress field, the maximum subsidence of the roof before the support is 817 mm, the maximum displacement of the two sides is 1780 mm, and the bottom heave is seriously damaged. The vertical displacement of the surrounding rock at the two vertex corners exceeds 700 mm; the maximum subsidence of the top and bottom after support is 285 mm, and the displacement of the two sides is 640 mm. Comparing the effect before and after the support, the subsidence of the roof after the support is reduced by 80%, the maximum displacement of the two sides has been reduced by 65%. Therefore, it can be seen that the properties of the surrounding rock are improved after the support, and the overall strength of the surrounding rock is increased as a whole, which effectively suppresses the deformation of the two sides of the roadway and is beneficial to the stability of the surrounding rock of the roadway.

5. Industrial Test

Because it is found that the effect of supporting haulage gateway is good, and in order to analyze the deformation law of surrounding rock and verify the rationality of composite bearing stress arch structure theory, relevant industrial tests are carried out. The roadway monitoring arrangement is "cross-point method," which means that anchor measuring points are buried on two-sides and the roof and floor of the roadway, and the distance change between the two points is measured by monitoring equipment. The comprehensive monitoring station (30 m away from each monitoring station) is arranged at 200 m from the opening of the transportation chute to observe the convergence deformation of the surrounding rock. It is found that the support effect is good, and the deformation of the surrounding rock of the roadway is effectively controlled. The layout of the monitoring points is shown in Figure 12, and construction site diagram of roadway after support is shown in Figure 13.

As shown in Figure 14 that the roadway deformation and surface displacement after support are observed for 36 days, and a total of 4 monitoring points (no. 1#, 2#, 3#, and 4#) are carried out, each data collection is carried out after mining; among them, the maximum convergence deformation of the two side walls of the roadway is 640 mm, and the maximum convergence deformation of the roof and floor of the roadway is 287 mm, and the initial deformation increases and gradually tends to be stable after reaching the maximum value. After the roadway is supported by anchor bolt and anchor cable, the integrity of surrounding rock is strengthened, the bulge of roadway side is effectively controlled, and the control effect of steel beam on roof is not obvious. It shows that the anchor bolt and anchor cable support parameters are reasonable, the surrounding rock control is remarkable, and the support system is good.

6. Conclusions

(1) With the collapse stability of working-face, after roadway excavation, the narrow coal pillar can be divided into three failure zones: fractured zone, plastic softening zone, and plastic hardening zone. A small structural stress arch mechanical model based on arch axis is established. Through the analysis of theoretical mechanical model and field actual

conditions, it is found that reasonable support methods can be selected to control the development of roadway plastic failure zone

(2) According to the site geological conditions, the stress arch height of the small structure of the surrounding rock of the transportation channel is determined to be 10.738 m, and the length of the anchor cable is determined to be 7.3 m according to the relationship between the stress arch height and the roadway size, and the twice support technology is selected to ensure the stability of the roadway. Among them, the anchor mesh support is used for the primary support, and the ordinary long anchor cable and grouting anchor cable are used for the secondary support

(3) In order to verify the rationality of the support parameters and the strength of the composite bearing stress arch structure, a mechanical model of the composite bearing stress arch structure of surrounding rock is proposed. The elastic-plastic mechanics is used to deduce the composite bearing stress arch structure, and the expression of the relationship between the ultimate bearing strength is obtained. After the transportation channel support of 17236 island working-face in the north of Zhangji coal mine is calculated, the support resistance of the support structure reaches 8.36 MPa. The ultimate bearing capacity of the bearing structure can reach 29.193 MPa

(4) The field monitoring results show that after the support of composite bearing stress arch structure, the deformation area of surrounding rock along the transportation channel is stable, the maximum shrinkage of roadway top and bottom is 287 mm, and the displacement of two sides is 640 mm. With the increase of monitoring time, the deformation is gradually stable, which is conducive to the long-term stability of the transportation channel

Data Availability

The data used to support the findings of this study are available from the corresponding author upon request.

Conflicts of Interest

The authors declare that there are no conflicts of interest regarding the publication of this paper.

Acknowledgments

This research was supported by the National Natural Science Foundation of China (nos. 51874002 and 52174102), China Scholarship Council (no. 202108340064), and Natural Science Foundation of Heilongjiang Province (no. LH2019E087).

References

[1] M. C. He, H. P. Xie, S. P. Peng, S. P. Peng, and Y. D. Jiang, "Study on rock mechanics in deep mining engineering," *Chinese Journal of Rock Mechanics and Engineering*, vol. 24, no. 16, pp. 2803–2813, 2005.

[2] G. Wu, W. J. Yu, J. Zuo, and S. Du, "Experimental and theoretical investigation on mechanisms performance of the rock-coal-bolt (RCB) composite system," *International Journal of Mining Science and Technology*, vol. 30, no. 6, pp. 759–768, 2020.

[3] J. H. Xue and Q. S. Liu, "Surrounding rock stability control theory and support technique in deep rock roadway for coal mine," *Journal of the China Coal Society*, vol. 36, no. 4, pp. 535–543, 2011.

[4] J. B. Bai, W. L. Shen, G. L. Guo, X. Y. Wang, and Y. Yu, "Roof deformation, failure characteristics, and preventive techniques of gob-side entry driving heading adjacent to the advancing working face," *Rock Mechanics and Rock Engineering*, vol. 48, no. 6, pp. 2447–2458, 2015.

[5] M. Wang, J. B. Bai, X. Y. Wang, Y. Xu, Y. H. Guo, and J. L. Cao, "The surrounding rock deformation rule and control technique of the roadway driven along goaf and heading for adjacent advancing coal face (in Chinese)," *Mining Safety Engineering*, vol. 29, pp. 197–202, 2012.

[6] J. M. Xi, J. H. Mao, G. S. Yang, and J. F. Wang, "Method for determining rational pillar width in mining roadway along working-face," *Mining Safety Engineering*, vol. 25, no. 4, pp. 400–4003, 2008.

[7] F. K. Qi, Y. J. Zhou, Z. H. Cao, Q. Zhang, and N. Li, "Width optimization of narrow coal pillar of roadway driving along working-face in fully mechanized top coal caving face," *Mining Safety Engineering*, vol. 33, no. 3, pp. 475–480, 2016.

[8] J. P. Yang, "Rational width of narrow coal pillar and control technology of surrounding strata at roadway driven along working-face," *Journal of Liaoning Technical University: Natural Science*, vol. 32, no. 1, pp. 39–43, 2013.

[9] M. S. Gao, N. Zhang, and L. Cheng, "The reasonable coal pillar width determined of roadway driving along working-face," *Mine Press Ceil Manage*, vol. 3, pp. 4–7, 2004.

[10] J. Wang, H. Huang, X. Xie, and B. Antonio, "Void-induced liner deformation and stress redistribution," *Tunnelling and Underground Space Technology*, vol. 40, pp. 263–276, 2014.

[11] S. Zhang, X. Wang, G. Fan, D. Zhang, and C. Jianbin, "Pillar size optimization design of isolated island panel gob-side entry driving in deep inclined coal seam——case study of Pingmei no. 6 coal seam," *Journal of Geophysics and Engineering*, vol. 15, no. 3, pp. 816–828, 2018.

[12] Y. Ma and S. Zhong, "Study on the relationship between hydraulic support on the working face with large mining height and surrounding rock," *Advanced Materials Research*, vol. 328-330, pp. 1671–1674, 2011.

[13] C. J. Hou and X. H. Li, "Stability principle of big and small structures of rock surrounding roadway driven along working-face in fully mechanized top coal caving face," *Journal of China Coal Society*, vol. 26, 2001.

[14] R. Yang, Y. Li, D. Guo, L. Yao, T. Yang, and T. Li, "Failure mechanism and control technology of water-immersed roadway in high- stress and soft rock in a deep mine," *International Journal of Mining Science and Technology*, vol. 27, no. 2, pp. 245–252, 2017.

[15] W. Wu, H. Zhu, J. S. Lin, X. Zhuang, and G. Ma, "Tunnel stability assessment by 3D DDA-key block analysis," *Tunnelling & Underground Space Technology*, vol. 71, pp. 210–214, 2018.

[16] N. Zhang, L. Yuan, C. Han, J. Xue, and J. Kan, "Stability and deformation of surrounding rock in pillarless gob-side entry retaining," *Safety Science*, vol. 50, no. 4, pp. 593–599, 2012.

[17] Y. F. Li and X. Z. Hua, "Mechanical analysis of stability of key blocks of overlying strata for gob-side entry retaining and calculating width of roadside backfill," *Rock and Soil Mechanics*, vol. 33, no. 4, pp. 1134–1140, 2012.

[18] M. S. Zhao, K. M. Wei, Z. K. Wen, and Y. L. Fang, "Study on the response of surrounding rock for gob-side entry retaining under the mining," *Applied Mechanics & Materials*, vol. 448, pp. 3879–3883, 2013.

[19] C. Q. Zhu, X. X. Miao, and Z. Liu, "Mechanical analysis on deformation of surrounding rock with road-in packing of gob-side entry retaining in fully-mechanized sub-level caving face," *Journal of Coal Science and Engineering (China)*, vol. 14, no. 1, pp. 24–28, 2008.

[20] Z. J. Wen, M. Rinne, Z. Z. Han, Z. Song, and Y. K. Shi, "Structure model of roadway with big deformation and its basic research into engineering theories," *Tehnicki Vjesnik*, vol. 21, no. 5, pp. 1065–1071, 2014.

[21] Q. Ma, Y. Tan, Z. Zhao, Q. Xu, J. Wang, and K. Ding, "Roadside support schemes numerical simulation and field monitoring of gob-side entry retaining in soft floor and hard roof," *Arabian Journal of Geosciences*, vol. 11, no. 18, pp. 1–13, 2018.

[22] S. Xie, E. Wang, D. Chen et al., "Failure analysis and control mechanism of gob-side entry retention with a 1.7-m flexible-formwork concrete wall: a case study," *Engineering Failure Analysis*, vol. 117, p. 104816, 2020.

[23] P. Yang, *Evolution Characteristics of Surrounding Rock Deformation of Gob-Side Entry Retaining in Deep Mine and Its Control Measures*, Anhui University of Science and Technology, 2018.

[24] L. Xuehua, *Surrounding Rock Stability Control Principle and Technology of Gob Side Entry Driving in Fully Mechanized Top Coal Caving*, China University of mining and Technology Press, 2008.

[25] B. Jianbiao, *Surrounding Rock Control of Gob Side Entry Driving*, China University of mining and Technology Press, 2006.

[26] H. Chaojiong and L. Xuehua, "Stability principle of big and small structures of rock surrounding roadway driven along working-face in fully mechanized top coal caving face," *China Coal Society*, vol. 26, pp. 1–6, 2001.

[27] W. Q. Xu, E. Y. Wang, R. X. Shen, D. Z. Song, and J. M. Zhang, "Distribution pattern of front abutment pressure of fully-mechanized working face of soft coal isolated island," *International Journal of Mining Science and Technology*, vol. 22, no. 2, pp. 279–284, 2012.

[28] W. J. Yu, G. S. Wu, B. An, and P. Wang, "Experimental study on the brittle-ductile response of a heterogeneous soft coal rock mass under multifactor coupling," *Geofluids*, vol. 2019, 15 pages, 2019.

[29] A. J. Das, P. K. Mandal, C. N. Ghosh, and A. Sinha, "Extraction of locked-up coal by strengthening of rib pillars with FRP - a comparative study through numerical modelling," *Mining Science and Technology*, vol. 27, no. 2, pp. 261–267, 2017.

[30] W. Li, J. Bai, S. Peng, X. Wang, and Y. Xu, "Numerical modeling for yield pillar design: a case study," *Rock Mechanics and Rock Engineering*, vol. 48, no. 1, pp. 305–318, 2015.

[31] M. C. He, H. S. Yuan, and H. W. Jing, *Theory and Practice of Bolt Supporting of Coal Mines in China*, Science Press, Beijing, 2004.

[32] Y. Zang, Z. J. Wan, F. C. Li et al., "Stability of coal pillar in gob-side entry driving under unstable overlying strata and its coupling support control technique," *International Journal of Mining Science and Technology*, vol. 23, no. 2, pp. 193–199, 2013.

[33] J. P. Zhang, L. M. Liu, J. Shao, and Q. H. Li, "Mechanical properties and application of right-hand rolling-thread steel bolt in deep and high-stress roadway," *Metals (Basel)*, vol. 9, no. 3, p. 346, 2019.

[34] G. X. Xie, J. Z. Li, L. Wang, and Y. Z. Tang, "Mechanical characteristics and time and space evolvement of stress shell in stope floor stratum," *Journal of the China Coal Society*, vol. 43, pp. 52–61, 2018.

[35] R. Pan, Q. Wang, B. Jiang et al., "Failure of bolt support and experimental study on the parameters of bolt- grouting for supporting the roadways in deep coal seam," *Engineering Failure Analysis*, vol. 80, pp. 218–233, 2017.

[36] X. X. Zhai, G. S. Huang, C. Y. Chen, and R. B. Li, "Combined supporting technology with bolt-grouting and floor pressure-relief for deep chamber: an underground coal mine case study," *Energies*, vol. 11, no. 1, p. 67, 2018.

[37] F. Xiao, G. Liu, Z. Zhang, Z. Shen, F. Zhang, and Y. Wang, "Acoustic emission characteristics and stress release rate of coal samples in different dynamic destruction time," *Mining Science and Technology*, vol. 26, no. 6, pp. 981–988, 2016.